Towards Causal Representation Learning with Observable Sources as Auxiliaries

Kwonho Kim [1] **Heejeong Nam** [2] **Inwoo Hwang** [3] **Sanghack Lee** [1]

Abstract

Causal representation learning seeks to uncover latent variables that generate observed data. A central challenge is identifiability, as infinitely many spurious solutions can exist. Prior works have relied on auxiliary variable assumptions that enforce conditional independence among latents. However, they require that auxiliary variables not be involved in the mixing function—a constraint that significantly limits the applicability in real-world settings. To address the issue, we study a more realistic setting where observed sources serve as auxiliary variables. We introduce a novel framework that selects proper auxiliaries to improve latent recoverability while satisfying identifiability conditions. To our knowledge, this is the first approach to establish identifiability in such a setting. By leveraging the graphical structure of latent variables, our method enhances both identifiability and disentanglement, pushing the boundaries of existing techniques in causal representation learning.

1. Introduction

Understanding the underlying generative process of observations is crucial for scientific discovery. Causal representation learning (CRL) seeks to uncover underlying latent variables from observed data. Such techniques have shown great promise in domains like healthcare (Sanchez et al., 2022), climate science (Yao et al., 2024a), and recommendation (Wang et al., 2022; 2024; Yang et al., 2024).

However, learning disentangled representations in an unsupervised manner remains theoretically difficult due to the existence of infinitely many indistinguishable solutions (Hyvärinen & Pajunen, 1999; Locatello et al., 2019). To address the problem, recent works have assumed conditional independence among latent sources given auxiliary variables, thereby enabling identifiability (Hyvärinen & Morioka, 2016; Khemakhem et al., 2020). Yet, this assumption is often unrealistic in practical settings where dependencies among sources naturally arise, such as in biological or physical systems (Cardoso, 1998; Theis, 2006).

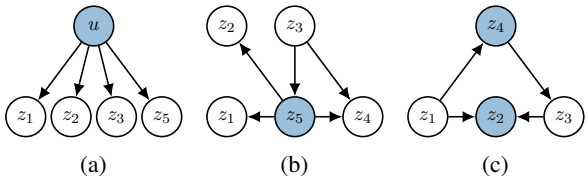

Figure 1: Examples of data generating process except mixing process, i.e. latent mechanism. Blue nodes represent the observable variables.

Recent advances have started relaxing this independence assumption by incorporating source dependencies into the model structure. Some methods assume specific parametric forms (Lu et al., 2022), while others take a non-parametric approach (Zheng & Zhang, 2023), yet they often overlook the potential of using observed sources entangled in the generative process itself as auxiliary information. This is a critical gap, as in many real-world scenarios, auxiliary variables may not be externally provided but rather embedded in the observations themselves.

In this work, we explore the novel setting where observed sources are used as auxiliaries to achieve identifiability. Motivated by systems governed by causal mechanisms—such as robotic arms—we show how observed sources and graphical information can aid in disentangling latent causes. By leveraging graphical structures and d-separation properties, we propose a framework for selecting auxiliary variables that enhance recoverability. Our empirical studies validate that the learned representations align with the conditional independencies implied by the latent causal graph.

2. Preliminary

In this section, we formally compare our setting with prior works using the following notation, and describe the objective of our problem formulation.

[1]Graduate School of Data Science, Seoul National University, Seoul, South Korea [2]Boeing Korea, Seoul, South Korea [3]Causal Artificial Intelligence Lab, Columbia University, New York, USA. Correspondence to: Sanghack Lee <sanghack@snu.ac.kr>.

Proceedings of the 42^{nd} International Conference on Machine Learning, Vancouver, Canada. PMLR 267, 2025.

2.1. Comparision of data generating process

Let $\mathbf{x} \in \mathbb{R}^m$ be an observation (e.g., image) which is generated from latent sources $\mathbf{z} \in \mathbb{R}^n$ with a mixing function g as follows:

$$\mathbf{x} = g(\mathbf{z}). \tag{1}$$

By adopting a Bayesian network, each latent source is generated as $z_i = f_i\big(\mathrm{Pa}_G(z_i), \epsilon_i\big), \quad \epsilon_i \sim p_{\epsilon_i}$ for all $i \in [n]$, where $\mathrm{Pa}_G(\cdot)$ denotes the parent nodes in a known causal graph $G = (V, E)$. The goal is to recover the independent components $\mathbf{z} = (z_1, \ldots, z_n)$ and the inverse function g^{-1} solely from observations $\mathbf{x}$. However, this is known to be unidentifiable with only i.i.d. samples (Hyvärinen & Pajunen, 1999). To deal with the problem, previous works assume conditional independence given auxiliary variables $\mathbf{u}$, such as class labels or time indices (Hyvarinen et al., 2019). They assume $\mathbf{u}$ has no direct effect on $\mathbf{x}$.

In contrast, we consider a more general setup where auxiliary variables may directly participate in the mixing function, rather than being restricted to external side information. Specifically, we treat auxiliary variables as observed latent sources $\mathbf{z}_o \subset \mathbf{z}$ that directly participate in the mixing function, where the generative process is governed by a DAG $\mathcal{G}$ capturing arbitrary dependencies. While CRL also accommodates dependencies among latents, it remains unclear how to effectively incorporate observed sources in that framework. The details for related work are provided in the Appendix A.

2.2. Problem formulation

Our goal is to establish the identifiability of the independent latent sources (i.e., $\mathbf{z}_{c_i}$) up to certain subspace-wise invertible transformation and permutation, given the observations $\mathbf{x}$, observed sources $\mathbf{z}_o (\subseteq \mathbf{z})$, and the latent Bayesian network $\mathcal{G}$ which encodes the conditional independence relationships between the latent sources as shown in Fig. 1.

Formally, we can partition unobserved sources into conditionally independent subsets $\mathbf{z}_{c_i}$ such that $\bigcup_{i=1}^{d} \mathbf{z}_{c_i} = \{z_1, \ldots, z_n\}$:

$$p(\mathbf{z}_o^- \mid \mathbf{z}_o) = \prod_{j=1}^{d} p\big(\mathbf{z}_{c_j} \mid \mathbf{z}_o\big), \tag{2}$$

where $\mathbf{z}_o$ are observed sources and $\mathbf{z}_o^-$ are unobserved.

The knowledge of the latent Bayesian network $\mathcal{G}$ allows us to leverage diverse conditional independence relationships between the sources. Importantly, the partition of the latent sources into subspaces $\mathbf{z}_{o^-} = \cup_i \mathbf{z}_{c_i}$ determines the *degree* of the identifiability we could achieve (Thm. 4.3 of Zheng & Zhang (2023)). Therefore, it is crucial to capture the proper observed sources $\mathbf{z}_u \subseteq \mathbf{z}_o$ that entails fine-grained subspaces $\mathbf{z}_{c_j}$ mutually independent to each other conditioned on $\mathbf{z}_u$.

3. Method

We establish identifiability in the presence of observed sources (Sec. 3.1). Based on conditions for identifiability, we introduce a framework with a graphical criterion to effectively leverage auxiliary variables that makes the conditionally independent latents more fine-grained (Sec. 3.2) and method to recover unobserved latents (Sec. 3.3).

3.1. Identifiability

To deal with problems that the observed sources $\mathbf{z}_o$ are included in the mixing function, we assume that the mixing function is constrained to a specific form as Yang et al. (2022).

Proposition 3.1. *Suppose the following assumptions hold:*
1. The observed data and sources are generated from Eq. (1) and Eq. (2)

2. The mixing function g is volume-preserving, i.e., $|det(\mathbf{J}_g(\mathbf{z}))| = 1$

3. For every value of $\mathbf{z}_{o^-}$, there exists $2d$ values of $\mathbf{z}_o$, such that the $2d$ vectors $\mathbf{w}(\mathbf{z}_{o^-}, \mathbf{z}_{o_i})$ are linearly independent, where vector $\mathbf{w}(\mathbf{z}_{o^-}, \mathbf{z}_{o_i})$ is defined as follows:

$$\mathbf{w}(\mathbf{z}_{o^-}, \mathbf{z}_{o_i}) = \big(\mathbf{v}(\mathbf{z}_{c_1}, \mathbf{z}_{o_i}), \ldots, \mathbf{v}(\mathbf{z}_{c_d}, \mathbf{z}_{o_i}), \mathbf{v}'(\mathbf{z}_{c_1}, \mathbf{z}_{o_i}), \ldots, \mathbf{v}'(\mathbf{z}_{c_d}, \mathbf{z}_{o_i})\big)$$

where

$$\mathbf{v}(\mathbf{z}_{c_j}, \mathbf{z}_{o_i}) = \left(\frac{\partial \log p(\mathbf{z}_{c_j} | \mathbf{z}_{o_i})}{\partial z_{c_j}^{(l)}}, \ldots, \frac{\partial \log p(\mathbf{z}_{c_j} | \mathbf{z}_{o_i})}{\partial z_{c_j}^{(h)}}\right),$$

$$\mathbf{v}'(\mathbf{z}_{c_j}, \mathbf{z}_{o_i}) = \left(\frac{\partial^2 \log p(\mathbf{z}_{c_j} | \mathbf{z}_{o_i})}{\partial (z_{c_j}^{(l)})^2}, \ldots, \frac{\partial^2 \log p(\mathbf{z}_{c_j} | \mathbf{z}_{o_i})}{\partial (z_{c_j}^{(h)})^2}\right)$$

and $\mathbf{z}_{c_j} = (z_{c_j^{(l)}}, \ldots, z_{c_j^{(h)}})$.

Then all the components of $\mathbf{z}_{o^-}$ (i.e., $\mathbf{z}_{c_i}$ where $c_i \in \{c_1, \ldots, c_d\}$) is identifiable up to a subspace-wise invertible transformation and a subspace-wise permutation.

Most prior CRL works assume a fixed mixing function across environments, enabling identifiability by canceling Jacobian log-determinant terms when differencing log-likelihoods across domains. In our setting, however, the mixing function varies with the observed source (e.g., domain label), breaking this cancellation and invalidating the standard proof. To overcome the issue, we assume the mixing is volume-preserving—i.e., the Jacobian determinant is always 1—so the log-determinant term becomes zero, restoring identifiability. Full details are provided in Appendix B.

Algorithm 1 Selection on Observables

Input: graph G, observed set O
Output: conditioning set C
$C \leftarrow \{$nodes acting only as confounders on $G\}$
$O \leftarrow O \setminus \{$nodes acting only as colliders on $G\}$
$max \leftarrow 0$
for each subset $T \subseteq O$ **do**
  $S \leftarrow Partition(G, T, O)$
  if $|S| > max$ **or** ($|S| = max$ **and** $|T| < |C|$) **then**
    $max \leftarrow |S|$
    $C \leftarrow T$
  end if
end for
return C

3.2. Selection on observables

According to the Prop. 3.1, the conditional independence determines the number of recoverable sources in the identifiability of latent variables and our goal is first to capture mutually independent groups of nodes given observed sources and the known causal graph. However, a naive approach of leveraging all observed sources might not capture conditional independence relationships, i.e., $z_1 \not\perp\!\!\!\perp z_3 \mid z_2, z_4$ in Fig. 1c. We propose a strategy that selects the most fine-grained conditionally independent groups of the latents with the minimum set of observed sources in Alg. 1. The algorithm initializes a candidate set by including only nodes that act as confounders and excluding those that act solely as colliders, in order to account for nodes that may serve as both. The *Partition* algorithm counts the number of groups that satisfy conditional independence by running *Bayes-ball* (Shachter, 1998) algorithm repeatedly. Finally, the algorithm outputs the conditioning set that results in the largest number of groups, i.e., the most fine-grained partitioning conditioned on proper observed sources $\mathbf{z}_u$. The detailed algorithm is provided in the Appendix C.

3.3. Learning to recover

To construct a representation that satisfies the identifiability conditions in Prop. 3.1, we enforce volume preservation in the encoder by adopting General Incompressible-flow Network (GIN) (Sorrenson et al., 2020) as our encoder. In addition to volume preservation, we also impose a graphical constraint via a structural neural network to preserve dependencies among latent variables that are not assumed to be independent, reflecting the known latent causal structure to strengthen disentanglement.

Volume-preservation While GIN originally optimizes only the log-likelihood of the conditional distribution given the auxiliary variables, we factorize the log-likelihood of the distribution as follows:

$$\log p_{\hat{g}^{-1}}(\mathbf{x}) = \log p(\hat{\mathbf{z}}) = \log p(\mathbf{z}_u) + \sum_i \log p(\hat{\mathbf{z}}_{u_i^-} \mid \mathbf{z}_u),$$

where $\hat{\mathbf{z}}_{u_i^-} = \hat{\mathbf{z}} \setminus \hat{\mathbf{z}}_{u_i}$. By factorizing the log-likelihood of the distribution, we can naturally address the issue that the information from the auxiliary variable is directly entangled with the observations. The preceding term will serve to absorb information about $\mathbf{z}_u$ from $\mathbf{x}$ while the latter term enforces the components of $\mathbf{z}_{u^-}$ to be independent given $\mathbf{z}_u$ by modeling them as a multivariate normal distribution with zero off-diagonal elements.

Graphical constraint Besides, $\hat{\mathbf{z}}_{u^-}$ contain the information of sources that are observed but not selected (expressed as $\mathbf{z}_n$). We need to keep the relationship between $\hat{\mathbf{z}}_n$ and ohter sources (regardless of whether they are observed or not) which is not independent. See relationship between z_2 and z_1, z_3 in Fig. 1c.

To deal with the problem, we leverage the structural neural net to enforce the relationship between other sources and $\hat{\mathbf{z}}_n$. A structural neural network is designed based on the latent graph $\mathcal{G}$ and not selected label $\mathbf{z}_n$. Specifically, $\mathbf{z}_n$ is predicted by arbitrary dimensions of $\hat{\mathbf{z}}_{u^-}$ working as parents of $\mathbf{z}_n$. Since we do not know exactly which dimension of the representation corresponds to which true latent variable, we rely only on the number of parents of $\mathbf{z}_n$. For example, in Fig. 1c, true z_2 is predicted by the certain dimension of the estimated representation given the other dimensions $(\hat{z}_1, \hat{z}_3)$, naturally reflecting the causal structure. The full objective function is:

$$\mathcal{L}(\theta) = \mathbb{E}\Bigg[\log p(\mathbf{z}_u) + \sum_i \log p(\hat{\mathbf{z}}_{u_i^-} \mid \mathbf{z}_u) + \log p(\mathbf{z}_n \mid \mathrm{Pa}^{\mathcal{G}}(\mathbf{z}_n))\Bigg]. \tag{3}$$

4. Experiment

We conduct experiments to empirically validate the our proposed method in leveraging observed sources.

4.1. Experimental Setup

Data and Metrics The data was generated using a Structural Causal Model (SCM) where each variable is determined by a linear combination of its parents and an additive noise term. Details are in Appendix D

To further demonstrate the effectiveness of our method on high-dimensional data, we used the Pendulum and modified Flow datasets Yang et al. (2021), which consist of structured, systematically sampled image data. Corresponding latent

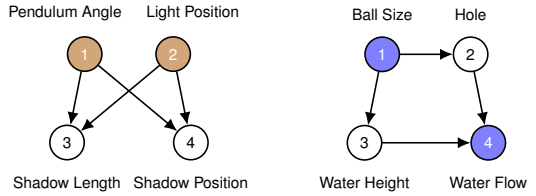

(a) Pendulum System (b) Flow System

Figure 2: Causal graphs for two systems. Colored nodes are observed sources: (a) Pendulum and (b) Flow.

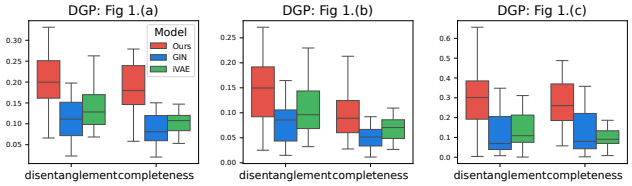

Figure 3: Comparison plot for DCI metric between Ours, GIN, and iVAE.

causal graphs are shown in Fig. 2. The implementation details is in Appendix D. After training the proposed method, to assess how well the learned representation aligns with the independence structure of the underlying graph, we measure Disentanglement, Completeness, Informativeness (DCI) metric (Eastwood & Williams, 2018) based on Mean Correlation Coefficient (MCC) matrix which is a widely accepted metric in the literature for measuring the degree of identifiability (Hyvärinen & Morioka, 2016). All the metrics are measured over 20 repetitions.

4.2. Empirical Results

Effectiveness of architecture To verify the effectiveness of our proposed architecture, we choose GIN (Sorrenson et al., 2020) and iVAE (Khemakhem et al., 2020) as baseline models. GIN is used as the encoder in our architecture, ensuring the volume-preserving property but not designed to handle observed sources. iVAE is also not designed to handle partially observed sources. Furthermore, it does not impose any constraints on the mixing function and solely relies on a multivariate normal distribution as the prior, ensuring that each latent variable is conditionally factorizable. For a fair comparison, all experiments are conducted using the same auxiliary variables filtered through the selection procedure.

Fig. 3 demonstrates that our proposed method outperforms other approaches in terms of the DCI metric. Our proposed method maximizes the likelihood of a conditionally factorizable distribution for the remaining components while simultaneously excluding the information of auxiliary variables mixed with the observation $\mathbf{x}$. This prevents spurious correlations in the representation by ensuring that the information of $\mathbf{z}_u$, which is related to unobserved latents, does not mix into the representation.

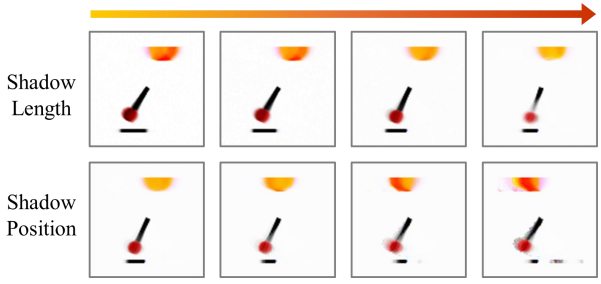

Figure 4: Latent traversal results for unobserved variables. The upper and lower rows show reconstructed images by traversing the variables for shadow length and shadow position, respectively.

Latent Traverse For better comprehensibility, we further extend our model to the image reconstruction task and perform latent traversal to assess whether the factors have been disentangled effectively. We conducted experiments on the pendulum dataset as shown in Fig. 2a, choosing the pendulum angle and light position as selected variables. To efficiently extract relevant features from high-dimensional image data and visualize disentangled factors, an extra encoder-decoder architecture with an additional MSE (Mean Squared Error) loss was adopted to ensure successful compression and reconstruction of the images.

Fig. 4 presents the results of generating counterfactual images by traversing unobserved latent variables after training our model with the reconstruction objective. As shown in the upper row, traversing the variable associated with shadow length gradually decreases its extent in the reconstructed images. Similarly, modifying the latent variable corresponding to shadow position causes the shadow to shift progressively to the right while mostly preserving the other factors. The successful disentanglement of unobserved latent variables further demonstrates the model's effectiveness in its transferability. More experimental results in Appendix E.

5. Conclusion

CRL aims to uncover latent variables in real-world systems. Our work is the first to achieve identifiability with observed sources by incorporating auxiliary variables into the mixing function. We also introduce a framework for selecting auxiliary variables to improve recoverability by leveraging the causal structure. Empirical results show that our method outperforms others in identifying true latent variables and reducing spurious correlations.

References

Cardoso, J.-F. Multidimensional independent component analysis. In *Proceedings of the 1998 IEEE International Conference on Acoustics, Speech and Signal Processing, ICASSP '98 (Cat. No.98CH36181)*, volume 4, pp. 1941–1944 vol.4, 1998. doi: 10.1109/ICASSP.1998.681443.

Eastwood, C. and Williams, C. K. I. A framework for the quantitative evaluation of disentangled representations. In *International Conference on Learning Representations*, 2018. URL https://openreview.net/forum?id=By-7dz-AZ.

Geiger, D., Verma, T., and Pearl, J. d-separation: From theorems to algorithms. In HENRION, M., SHACHTER, R. D., KANAL, L. N., and LEMMER, J. F. (eds.), *Uncertainty in Artificial Intelligence*, volume 10 of *Machine Intelligence and Pattern Recognition*, pp. 139–148. North-Holland, 1990.

Hyvärinen, A. and Morioka, H. Unsupervised feature extraction by time-contrastive learning and nonlinear ica. In Garnett, R., Lee, D., von Luxburg, U., Guyon, I., and Sugiyama, M. (eds.), *Advances in Neural Information Processing Systems*, number NIPS 2016 in Advances in neural information processing systems, pp. 3772–3780, United States, 2016. Neural Information Processing Systems Foundation. Annual Conference on Neural Information Processing Systems, NIPS ; Conference date: 05-12-2016 Through 10-12-2016.

Hyvärinen, A. and Pajunen, P. Nonlinear independent component analysis: existence and uniqueness results. *Neural Netw.*, 12(3), 1999.

Hyvarinen, A., Sasaki, H., and Turner, R. Nonlinear ica using auxiliary variables and generalized contrastive learning. In Chaudhuri, K. and Sugiyama, M. (eds.), *Proceedings of the Twenty-Second International Conference on Artificial Intelligence and Statistics*, volume 89 of *Proceedings of Machine Learning Research*, pp. 859–868. PMLR, 16–18 Apr 2019.

Khemakhem, I., Kingma, D., Monti, R., and Hyvarinen, A. Variational autoencoders and nonlinear ica: A unifying framework. In Chiappa, S. and Calandra, R. (eds.), *Proceedings of the Twenty Third International Conference on Artificial Intelligence and Statistics*, volume 108 of *Proceedings of Machine Learning Research*, pp. 2207–2217. PMLR, 26–28 Aug 2020.

Kügelgen, J. V., Sharma, Y., Gresele, L., Brendel, W., Schölkopf, B., Besserve, M., and Locatello, F. Self-supervised learning with data augmentations provably isolates content from style. In Beygelzimer, A., Dauphin, Y., Liang, P., and Vaughan, J. W. (eds.), *Advances in Neural Information Processing Systems*, 2021. URL https://openreview.net/forum?id=4pf_pOo0Dt.

Li, A., Pan, E., and Bareinboim, E. Disentangled representation learning in non-markovian causal systems. Technical Report R-110, Causal Artificial Intelligence Lab, Columbia University, May 2024.

Liang, W., Kekić, A., von Kügelgen, J., Buchholz, S., Besserve, M., Gresele, L., and Schölkopf, B. Causal component analysis. In *Thirty-seventh Conference on Neural Information Processing Systems*, 2023.

Lippe, P., Magliacane, S., Löwe, S., Asano, Y. M., Cohen, T., and Gavves, E. Causal representation learning for instantaneous and temporal effects in interactive systems. In *The Eleventh International Conference on Learning Representations*, 2023.

Locatello, F., Bauer, S., Lučić, M., Rätsch, G., Gelly, S., Schölkopf, B., and Bachem, O. F. Challenging common assumptions in the unsupervised learning of disentangled representations. In *International Conference on Machine Learning*, 2019. Best Paper Award.

Lu, C., Wu, Y., Hernández-Lobato, J. M., and Schölkopf, B. Invariant causal representation learning for out-of-distribution generalization. In *International Conference on Learning Representations*, 2022. URL https://openreview.net/forum?id=-e4EXDWXnSn.

Pan, Y. and Bareinboim, E. Counterfactual image editing. In *Proceedings of the 41st International Conference on Machine Learning (ICML)*, 2024. URL https://openreview.net/forum?id=OXzkw7vFIO.

Pearl, J. *Causality: Models, Reasoning and Inference*. Cambridge University Press, 2nd edition, 2009.

Sanchez, P., Voisey, J. P., Xia, T., Watson, H. I., O'Neil, A. Q., and Tsaftaris, S. A. Causal machine learning for healthcare and precision medicine. *Royal Society Open Science*, 9(8):220638, 2022.

Shachter, R. D. Bayes-ball: Rational pastime (for determining irrelevance and requisite information in belief networks and influence diagrams). In *Proceedings of the Fourteenth Conference on Uncertainty in Artificial Intelligence*, UAI'98, pp. 480–487, San Francisco, CA, USA, 1998. Morgan Kaufmann Publishers Inc. ISBN 155860555X.

Sorrenson, P., Rother, C., and Köthe, U. Disentanglement by nonlinear ica with general incompressible-flow networks (gin), 2020. URL https://arxiv.org/abs/2001.04872.

Theis, F. Towards a general independent subspace analysis. In Schölkopf, B., Platt, J., and Hoffman, T. (eds.), *Advances in Neural Information Processing Systems*, volume 19. MIT Press, 2006. URL https://proceedings.neurips.cc/paper_files/paper/2006/file/20479c788fb27378c2c99eadcf207e7f-Paper.pdf.

Wang, S., Chen, X., and Yao, L. On causally disentangled state representation learning for reinforcement learning based recommender systems. In *Proceedings of the 33rd ACM International Conference on Information and Knowledge Management*, pp. 2390–2399, 2024.

Wang, W., Lin, X., Feng, F., He, X., Lin, M., and Chua, T.-S. Causal representation learning for out-of-distribution recommendation. In *Proceedings of the ACM Web Conference 2022*, pp. 3562–3571, 2022.

Yang, M., Liu, F., Chen, Z., Shen, X., Hao, J., and Wang, J. Causalvae: Disentangled representation learning via neural structural causal models. In *Proceedings of the IEEE/CVF conference on computer vision and pattern recognition*, pp. 9593–9602, 2021.

Yang, X., Wang, Y., Sun, J., Zhang, X., Zhang, S., Li, Z., and Yan, J. Nonlinear ICA using volume-preserving transformations. In *International Conference on Learning Representations*, 2022. URL https://openreview.net/forum?id=AMpki9kp8Cn.

Yang, X., Li, X., Liu, Z., Wang, Y., Lu, S., and Liu, F. Disentangled causal representation learning for debiasing recommendation with uniform data. *Applied Intelligence*, pp. 1–16, 2024.

Yao, D., Muller, C., and Locatello, F. Marrying causal representation learning with dynamical systems for science. *arXiv preprint arXiv:2405.13888*, 2024a.

Yao, D., Xu, D., Lachapelle, S., Magliacane, S., Taslakian, P., Martius, G., von Kügelgen, J., and Locatello, F. Multi-view causal representation learning with partial observability. In *The Twelfth International Conference on Learning Representations*, 2024b.

Zhang, K., Xie, S., Ng, I., and Zheng, Y. Causal representation learning from multiple distributions: A general setting. In *Forty-first International Conference on Machine Learning*, 2024.

Zheng, Y. and Zhang, K. Generalizing nonlinear ICA beyond structural sparsity. In *Thirty-seventh Conference on Neural Information Processing Systems*, 2023.

Appendix

A. discussion

Related Work One of the key obstacles in CRL is the dependence among latent sources induced by underlying causal mechanisms. It directly violates the assumption of conditionally independent sources, which underlies the identifiability of many nonlinear ICA approaches that rely on conditionally factorized priors (Khemakhem et al., 2020). To address this issue, several works explicitly incorporate a known or assumed causal graph over the latent variables to model source dependencies. For example, Yang et al. (2021) (CausalVAE) propose a structured variational autoencoder where the latent variables follow a predefined causal DAG, enabling do-interventions in the latent space. Similarly, Pan & Bareinboim (2024) (ANCM) handle non-Markovian generative processes by modeling image generation with an augmented causal graph that captures temporally entangled latent factors. While these methods provide a framework for incorporating causal structure into representation learning, they operate under a fully supervised setting, assuming access to structured semantic labels or ground-truth causal factors. Moreover, they are primarily focused on image generation and counterfactual editing tasks, rather than the general identifiability or recovery of latent sources from more weakly supervised or observational data.

To achieve identifiability under such dependencies, many methods rely on interventional data which can be impractical in real-world settings (Lippe et al., 2023; Liang et al., 2023; Li et al., 2024). In particular, the Liang et al. (2023) (CauCa) assumes a Markovian graph and leverages interventions for identifiability, while Li et al. (2024) (CRID) handles more general non-Markovian settings by explicitly modeling unobserved confounders. Both of CauCA and CRID share with our approach the use of causal graph to guide recovery, suggesting that our method could be extended to non-Markovian settings in future work.

As an alternative, recent efforts have aimed to prove identifiability from observational data alone. For example, Yao et al. (2024b) introduce a method based on block-identifiability (Kügelgen et al., 2021), which extracts shared latent variables from multiple views using contrastive learning and entropy regularization. Zhang et al. (2024) show that assuming structural sparsity among the sources enables identifiability without any explicit causal graph. While these works relax assumptions on data collection, they rely on indirect structural constraints. In contrast, we investigate how to select or exploit observed sources as auxiliary variables under a known causal structure to recover latent sources. This approach retains the strengths of causal modeling while improving recoverability in settings where full interventions or disentangled views are unavailable.

Nonlinear ICA Nonlinear ICA considers independent latent sources, i.e.,

$$p(\mathbf{z}) = \prod_{i=1}^{n} p(z_i). \tag{4}$$

To deal with the case of Fig. 1b, we can partition the latent sources into conditionally independent sets, $\mathbf{z}_{c_i} (i = 1, ..., d)$ where $\cup_{i=1}^{d} \mathbf{z}_{c_i} = \{z_1, \ldots, z_n\}$. It enables a more general formulation of Eq. (4) as Zheng & Zhang (2023):

$$p_{\mathbf{z}|\mathbf{u}}(\mathbf{z}|\mathbf{u}) = \prod_{i=1}^{n_i} p_{z_i}(z_i) \prod_{j=1}^{d} p_{\mathbf{z}_{c_j}|\mathbf{u}}(\mathbf{z}_{c_j}|\mathbf{u}). \tag{5}$$

where n_i is the number of mutually independent sources. Zheng & Zhang (2023) partition all the sources into a set of mutually independent sources $\mathbf{z}_I$ and a set of variables in which do not need to be independent $\mathbf{z}_{o^-} = \cup_{i=1}^{d} \mathbf{z}_{c_i}$. In Eq. (2), we further generalize Eq. (5) into the setting with observed sources, which includes Eq. (5) as a special case in that $\mathbf{u}$ is independent from DGP.

$$p_{\mathbf{z}_{o^-}|\mathbf{z}_o}(\mathbf{z}_{o^-}|\mathbf{z}_o) = \prod_{i=1}^{n_i} p_{z_i}(z_i) \prod_{j=1}^{d} p_{\mathbf{z}_{c_j}|\mathbf{z}_o}(\mathbf{z}_{c_j}|\mathbf{z}_o). \tag{6}$$

where $\mathbf{z}_o$ is observed sources and $\mathbf{z}_{o^-}$ is unobserved sources. The former term corresponds to the case without auxiliary variables, which is beyond the scope of our study and thus not considered further.

B. Theoretical Anlaysis

Firstly, we begin with the definition of identifiability, which is the goal of nonlinear ICA and causal representation learning. By adopting a Structural Causal Model (SCM, (Pearl, 2009)), we represent a data-generating process regarding latent

sources as

$$z_i = f_i(\mathrm{Pa}^{\mathcal{G}}(z_i), \epsilon_i), \quad \epsilon_i \sim p_{\epsilon_i}, \tag{7}$$

for all $i \in [n]$ where $\mathrm{Pa}^{\mathcal{G}}(\cdot)$ represents parent nodes on a latent causal graph $\mathcal{G}$ consisting of nodes V and edges E.

Definition B.1. (Identifiability). Suppose the observations $\mathbf{x}$ are generated by true latent mechanism specified by $\Theta = (\mathbf{f}, p(\boldsymbol{\epsilon}), \mathbf{g})$ given in Eqs. (1) and (7). The learned generative model parameterized by $\hat{\Theta} = \left(\hat{\mathbf{f}}, \hat{p}(\boldsymbol{\epsilon}), \hat{\mathbf{g}}\right)$ is observationally equivalent to the true model if the model distribution $p_{\hat{\Theta}}(\mathbf{x})$ matches the data distribution $p_{\Theta}(\mathbf{x})$ for any value of $\mathbf{x}$. Let A be an arbitrary invertible transformation. We say that the model is identifiable up to A if

$$p_{\hat{\Theta}}(\mathbf{x}) = p_{\Theta}(\mathbf{x}) \implies \hat{\mathbf{g}} = \mathbf{g} \circ A. \tag{8}$$

Once the mixing function g is identified, the latent variables can be identified up to A:

$$\begin{aligned} \hat{\mathbf{z}} = \hat{\mathbf{g}}^{-1}(\mathbf{x}) &= (A^{-1} \circ \mathbf{g}^{-1})(\mathbf{x}) \\ &= A^{-1}(\mathbf{g}^{-1}(\mathbf{x})) \\ &= A^{-1}(\mathbf{z}). \end{aligned}$$

The following proposition is a restatement of theorem of Zheng & Zhang (2023) under our setting. It addresses the case where the auxiliary variable is not included in the mixing function, which corresponds to the setting of conventional nonlinear ICA and CRL.

Proposition B.2. *Suppose the following assumptions hold:*

1. *The observed data and sources are generated from Eq. (1) and Eq. (2)*
2. *The observable sources do not have direct edge into the observation* $\mathbf{x}$*, i.e.,* $\frac{\partial \mathbf{x}}{\partial \mathbf{z}_o} = 0$
3. *For every value of* $\mathbf{z}_D$*, there exists* $2d+1$ *values of* $\mathbf{z}_o$*, such that the* $2d$ *vectors* $\mathbf{w}(\mathbf{z}_D, \mathbf{z}_{o_i}) - \mathbf{w}(\mathbf{z}_D, \mathbf{z}_{o_0})$ *are linearly independent, where vector* $\mathbf{w}(Z_D, \mathbf{z}_{o_i})$ *is defined as follows:*

$$\begin{aligned} \mathbf{w}(\mathbf{z}_D, \mathbf{z}_{o_i}) = \big(&\mathbf{v}(\mathbf{z}_{c_1}, \mathbf{z}_{o_i}), \ldots, \mathbf{v}(\mathbf{z}_{c_d}, \mathbf{z}_{o_i}), \\ &\mathbf{v}'(\mathbf{z}_{c_1}, \mathbf{z}_{o_i}), \ldots, \mathbf{v}'(\mathbf{z}_{c_d}, \mathbf{z}_{o_i})\big) \end{aligned}$$

where

$$\begin{aligned} \mathbf{v}(\mathbf{z}_{c_j}, \mathbf{z}_{o_i}) &= \left(\frac{\partial \log p(\mathbf{z}_{c_j} \mid \mathbf{z}_{o_i})}{\partial z_{c_j}^{(l)}}, \ldots, \frac{\partial \log p(\mathbf{z}_{c_j} \mid \mathbf{z}_{o_i})}{\partial z_{c_j}^{(h)}}\right), \\ \mathbf{v}'(\mathbf{z}_{c_j}, \mathbf{z}_{o_i}) &= \left(\frac{\partial^2 \log p(\mathbf{z}_{c_j} \mid \mathbf{z}_{o_i})}{\partial (z_{c_j}^{(l)})^2}, \ldots, \frac{\partial^2 \log p(\mathbf{z}_{c_j} | \mathbf{z}_{o_i})}{\partial (z_{c_j}^{(h)})^2}\right) \end{aligned}$$

and $\mathbf{z}_{c_j} = (z_{c_j^{(l)}}, \ldots, z_{c_j^{(h)}})$.

Then all components of $\mathbf{z}_D$ *(i.e.,* $\mathbf{z}_{c_i}$ *where* $c_i \in \{c_1, \ldots, c_d\}$*) is identifiable up to a subspace-wise invertible transformation and a subspace-wise permutation.*

Proof. Let $h : \mathbf{z}_{o^-} \to \hat{\mathbf{z}}_{o^-}$ denote the transformation from true sources to estimated sources. Thus, we can derive $\hat{g} = g \circ h^{-1}(\mathbf{z}_{o^-})$ equivalently as

$$\mathbf{J}_g(\mathbf{z}_{o^-}) = \mathbf{J}_{\hat{g} \circ h}(\mathbf{z}_{o^-}) = \mathbf{J}_{\hat{g}}(\hat{\mathbf{z}}_{o^-}) \mathbf{J}_h(\mathbf{z}_{o^-})$$

by using chain rule repeatedly. $\mathbf{J}_h(\mathbf{z}_{o^-})$ must be invertible and have a non-zero determinant because $\mathbf{J}_{\hat{g}}(\hat{\mathbf{z}}_{o^-})$ and $\mathbf{J}_g(\mathbf{z}_{o^-})$ have full column rank. The change of variable rule and Assumption 2 make the following equations hold:

$$p(\mathbf{z}_{o^-} \mid \mathbf{z}_o) \cdot |\det(\mathbf{J}_{h^{-1}}(\hat{\mathbf{z}}_{o^-}))| = p(\hat{\mathbf{z}}_{o^-} \mid \mathbf{z}_o).$$

By taking logarithm on both sides, we can obtain

$$\log p(\mathbf{z}_{o^-} \mid \mathbf{z}_o) + \log |\det(\mathbf{J}_{h^{-1}}(\hat{\mathbf{z}}_{o^-}))| = \log p(\hat{\mathbf{z}}_{o^-} \mid \mathbf{z}_o).$$

According to the Assumption 1 and $\cup_i \mathbf{z}_{c_i} = \mathbf{z} \setminus \mathbf{z}_o$, the joint log densities can be factorized as

$$\sum_{j=c_1}^{c_d} \log p(\mathbf{z}_j \mid \mathbf{z}_o) + \log |\det(\mathbf{J}_{h^{-1}}(\hat{\mathbf{z}}_{o^-}))| = \sum_{j=c_1}^{c_d} \log p(\hat{\mathbf{z}}_j \mid \hat{\mathbf{z}}_o).$$

Thus, for $\mathbf{z}_o = \mathbf{z}_{o_0}, \dots \mathbf{z}_{o_{2d}}$, we have $2d+1$ equations. Subtracting each equation corresponding to $\mathbf{z}_{o_1}, \dots, \mathbf{z}_{o_2 d}$ with the equation corresponding to $\mathbf{z}_{o_0}$ results in $2d$ equations:

$$\sum_{i=c_1}^{c_d} (\log p(\mathbf{z}_i \mid \mathbf{z}_{o_j}) - \log p(\mathbf{z}_i \mid \mathbf{z}_{o_0})) = \sum_{i=c_1}^{c_d} (\log p(\hat{\mathbf{z}}_i \mid \mathbf{z}_{o_j}) - \log p(\hat{\mathbf{z}}_i \mid \mathbf{z}_{o_0})) \tag{9}$$

Take the derivatives of both sides of Eq. (9) with respect to $\hat{z}_k$ and $\hat{z}_v$ where $k, v \in \{1, \dots, n\}$ and they are not indices of the same subspace. It is clear that the RHS of Eq. (9) equals to zero because k and v are not indices of the same subspace. For the i-th term of the summation on the LHS, we can get following equations:

$$\begin{aligned} \sum_{l=i^{(l)}}^{i^{(h)}} \Bigg(& \left(\frac{\partial^2 \log p(\mathbf{z}_i \mid \mathbf{z}_{o_j})}{(\partial z_l)^2} - \frac{\partial^2 \log p(\mathbf{z}_i \mid \mathbf{z}_{o_0})}{(\partial z_l)^2} \right) \cdot \frac{\partial z_l}{\partial \hat{z}_k} \frac{\partial z_l}{\partial \hat{z}_v} \\ & + \left(\frac{\partial \log p(\mathbf{z}_i \mid \mathbf{z}_{o_j})}{\partial z_l} - \frac{\partial \log p(\mathbf{z}_i \mid \mathbf{z}_{o_0})}{\partial z_l} \right) \cdot \frac{\partial^2 z_l}{\partial \hat{z}_k \partial \hat{z}_v} \Bigg) = 0, \end{aligned} \tag{10}$$

where i_l and i_h are the minimum and maximum indices of elements in $\mathbf{z}_i = (z_{il}, \dots, z_{ih})$. By iterating i from c_1 to c_d, we can also iterate l from 0 to n. Thus, there exists a linear system with a $2d \times 2d$ coefficient matrix.

Considering Assumption 3, the coefficient matrix of the linear system has full rank. The only solution of Eq. (10) is $\frac{\partial z_l}{\partial \hat{z}_k} \frac{\partial z_l}{\partial \hat{z}_v} = 0$ and $\frac{\partial^2 z_l}{\partial \hat{z}_k \partial \hat{z}_v} = 0$. Note that $\frac{\partial z_l}{\partial \hat{z}_k}$ and $\frac{\partial z_l}{\partial \hat{z}_v}$ cannot be both zero because of invertibility of h. Therefore, k can only be the index of an estimated source from one independent subspace, which, together with the invertibility, leads to the conclusion that $\mathbf{z}_{o^-}$ is a composition of an invertible subspace-wise transformation and a subspace-wise permutation of $\hat{Z}_D$. So it is the mapping from $\hat{\mathbf{z}}_{o^-}$ to $\mathbf{z}_{o^-}$ since the subspace-wise transformation is invertible and the inverse of a block-wise permutation matrix is still a block-wise invertible matrix. □

We now establish identifiability in the presence of observable sources, where an auxiliary variable directly influences the observation $\mathbf{x}$ through the mixing function. This constitutes the proof of Prop. 3.1.

Proof. Assume observational equivalence between estimated and true model, i.e. $p_g(\mathbf{x}) = p_{\hat{g}}(\mathbf{x})$. The change of varialbe rule makes following equations to hold:

$$p(\mathbf{x}) = p(\mathbf{z}) \cdot |\det(\mathbf{J}_{g^{-1}})(\mathbf{x})| = p(\hat{\mathbf{z}}) \cdot |\det(\mathbf{J}_{\hat{g}^{-1}})(\mathbf{x})|$$

Since $p(\mathbf{z}) = p(\mathbf{z}_{o^-} \mid \mathbf{z}_o) \cdot p(\mathbf{z}_o)$,

$$p(\mathbf{z}_{o^-} \mid \mathbf{z}_o) \cdot p(\mathbf{z}_o) \cdot |\det(\mathbf{J}_{g^{-1}})(\mathbf{x})| = p(\hat{\mathbf{z}}_{o^-} \mid \hat{\mathbf{z}}_o) \cdot p(\hat{\mathbf{z}}_o) \cdot |\det(\mathbf{J}_{\hat{g}^{-1}})(\mathbf{x})|$$

also can hold. Note that $p(\hat{\mathbf{z}}_o)$ can be replaced by $p(\mathbf{z}_o)$ because $\mathbf{z}_o$ is already observed.

$$p(\mathbf{z}_{o^-} \mid \mathbf{z}_o) \cdot |\det(\mathbf{J}_{g^{-1}})(\mathbf{x})| = p(\hat{\mathbf{z}}_{o^-} \mid \mathbf{z}_o) \cdot |\det(\mathbf{J}_{\hat{g}^{-1}})(\mathbf{x})|$$

By taking logarithm on both sides, we can obtain

$$\log p(\mathbf{z}_{o^-} \mid \mathbf{z}_o) + \log |\det(\mathbf{J}_{g^{-1}})(\mathbf{x})| = \log p(\hat{\mathbf{z}}_{o^-} \mid \mathbf{z}_o) + \log |\det(\mathbf{J}_{\hat{g}^{-1}})(\mathbf{x})|.$$

According to the Assumption 1, Assumption 2 and $\cup_i \mathbf{z}_{c_i} = \mathbf{z} \setminus \mathbf{z}_o$, the joint log densities can be factorized as

$$\sum_{j=c_1}^{c_d} \log p(\mathbf{z}_j \mid \mathbf{z}_o) = \sum_{j=c_1}^{c_d} \log p(\hat{\mathbf{z}}_j \mid \mathbf{z}_o).$$

Thus, for $\mathbf{z}_o = \mathbf{z}_{o_0}, \dots \mathbf{z}_{o_{2d-1}}$, we have $2d$ equations. Take the derivatives of both sides of above equation with respect to $\hat{z}_k$ and $\hat{z}_v$ where $k, v \in \{1, \dots, n\}$ and they are not indices of the same subspace. It is clear that the RHS of Eq. (9) equals to zero because k and v are not indices of the same subspace. For the i-th term of the summation on the LHS, we can get following equations:

$$\sum_{l=i^{(l)}}^{i^{(h)}} \left(\left(\frac{\partial^2 \log p(\mathbf{z}_i \mid \mathbf{z}_o)}{(\partial z_l)^2} \right) \cdot \frac{\partial z_l}{\partial \hat{z}_k} \frac{\partial z_l}{\partial \hat{z}_v} + \left(\frac{\partial \log p(\mathbf{z}_i \mid \mathbf{z}_o)}{\partial z_l} \right) \cdot \frac{\partial^2 z_l}{\partial \hat{z}_k \partial \hat{z}_v} \right) = 0, \tag{11}$$

where i_l and i_h are the minimum and maximum indices of elements in $\mathbf{z}_i = (z_{il}, \dots, z_{ih})$. By iterating i from c_1 to c_d, we can also iterate l from 0 to n.

Considering Assumption 3, the coefficient matrix of the linear system has full rank. The only solution of Eq. (11) is $\frac{\partial z_l}{\partial \hat{z}_k} \frac{\partial z_l}{\partial \hat{z}_v} = 0$ and $\frac{\partial^2 z_l}{\partial \hat{z}_k \partial \hat{z}_v} = 0$. Note that $\frac{\partial z_l}{\partial \hat{z}_k}$ and $\frac{\partial z_l}{\partial \hat{z}_v}$ cannot be both zero because of invertibility of h. Therefore, k can only be the index of an estimated source from one independent subspace, which, together with the invertibility, leads to the conclusion that $\mathbf{z}_{o^-}$ is a composition of an invertible subspace-wise transformation and a subspace-wise permutation of $\hat{Z}_D$. So it is the mapping from $\hat{Z}_D$ to $\mathbf{z}_{o^-}$ since the subspace-wise transformation is invertible and the inverse of a block-wise permutation matrix is still a block-wise invertible matrix. □

C. Algorithm Details

Selection on Observables According to the Prop. 3.1, the conditional independence determines the number of recoverable sources in the identifiability of latent variables and our goal is first to capture mutually independent groups of nodes given observable sources and the known causal graph. However, a naive approach of leveraging all observed sources might not capture conditional independence relationships, i.e., $z_1 \not\perp\!\!\!\perp z_3 \mid z_2, z_4$ in Fig. 1c. It is necessary to capture a proper subset of observed sources that entails the most fine-grained groups of mutually independent sources, and ultimately, leads to the most granular identifiability.

Formally, we aim to discover a conditional independence structure that partition $\mathbf{z}_{o^-}$ into the most fine-grained subgroups such that:

$$\mathbf{z}_{c_i} \perp\!\!\!\perp \mathbf{z}_{c_j} \mid \mathbf{z}_u, \quad \text{for all } i \neq j, \tag{12}$$

where $\mathbf{z}_u \subseteq \mathbf{z}_o$, $\cup_i \mathbf{z}_{c_i} \subseteq \mathbf{z} \setminus \mathbf{z}_o$, and $\mathbf{z}_{c_i} \cap \mathbf{z}_{c_j} = \emptyset$ for all $i \neq j$. Importantly, satisfying a fine-grained conditional independence condition enables the identification of a greater number of latent variables. This ensures a more precise disentanglement of the underlying causal structure, leading to improved recoverability and manipulability of the true latent factors.

We propose a strategy that selects the most fine-grained conditionally independent groups of the latents with the minimum set of observed sources in Alg. 1. The algorithm initializes a candidate set by including only nodes that act as confounders and excluding those that act solely as colliders, in order to account for nodes that may serve as both. The *Partition* algorithm in Alg. 2 counts the number of groups that satisfy conditional independence by running *Bayes-ball* (Shachter, 1998) algorithm repeatedly. Finally, the algorithm outputs the conditioning set that results in the largest number of groups, i.e., the most fine-grained partitioning.

Example Consider the latent graph in the Fig. 1c. Observed set $O = \{z_2, z_4\}$. We will iterate all the subsets of O, i.e., $\{z_2\}, \{z_4\}, \{z_2, z_4\}$.[1] Firstly, with conditioning set $\{z_2\}$, the partition process is as follow:

1. Started from z_1, the *result* contains z_1.
2. *Bayes-ball* algorithm get input as $G, \{z_2\}$ and *result*.

[1] $\emptyset$ cannot be considered due to the condition for the identifiability.

Algorithm 2 Graph Partition by Conditional Independence

Input: graph $G = (\mathbf{V}, \mathbf{E})$, condition C, observed set O
Output: a set of d-connected node clusters R
$R \leftarrow \emptyset$
for each node n in $\mathbf{V} \setminus O$ **do**
  if $\exists_{\mathbf{C} \in R}\, n \in \mathbf{C}$ **then**
    continue
  end if
  $result \leftarrow \{n\}$;
  while $result$ updated **do**
    $result \leftarrow \textsc{BayesBall}(G, C, O, result)$
  end while
  Add $result$ to R
end for
return R

3. In the *Bayes-ball*, path from z_1 to z_3 through z_2 cannot be d-separated because z_2 works as collider.
4. The path from z_1 to z_3 also cannot be d-separated.
5. The *result* is $\{\{z_1, z_3\}\}$ except for observed source z_2.

With conditioning set $\{z_4\}$, by following same process, the *result* will be $\{\{z_1\}, \{z_3\}\}$. The conditioning set $\{z_2, z_4\}$ makes the result to be $\{\{z_1, z_3\}\}$. Hence, the selection result will be $\{z_4\}$ for the most fine-grained conditionally independent latents.

Bayes-Ball Algorithm The best known criterion for conditional independence is *d-separation* (Geiger et al., 1990). We want to find clusters with inter-cluster d-connectedness and intra-cluster d-separation.

We exploit *Bayes-ball* algorithm to examine the conditional independence of two node sets on the given graph $\mathcal{G}$. The Bayes-ball algorithm can be extended to partition graph. It returns a set of nodes dependent to an input node set.

D. Experimental Details

Metrics After training the proposed method, we measure Disentanglement, Completeness, Informativeness (DCI) metric (Eastwood & Williams, 2018) based on Mean Correlation Coefficient (MCC) matrix which is a widely accepted metric in the literature for measuring the degree of identifiability (Hyvärinen & Morioka, 2016). We assess how well the learned representation aligns with the independence structure of the underlying graph.

Specifically, the MCC matrix is defined as:

$$\mathbf{MCC}_{ij} = \text{corr}(z_i, \hat{z}_j), \tag{13}$$

where each entry $\mathbf{MCC}_{ij}$ represents the Pearson correlation coefficient between the true latent variable z_i and the estimated latent variable $\hat{z}_j$. The optimal permutation σ^* is selected to maximize the total correlation, ensuring that each estimated latent variable is matched to the most similar true latent variable.

Based on the computed MCC matrix, we evaluate models with Disentanglement and Completeness among DCI metrics:

$$D = 1 - H(P_{i,\cdot}), \tag{14}$$

$$C = 1 - H(P_{\cdot,j}), \tag{15}$$

where $P_{i,j}$ is the value from the MCC matrix, representing the contribution of the estimated latent variable $\hat{z}_j$ to the true latent factor z_i. The entropy function $H(\cdot)$ measures the dispersion of importance values across dimensions, ensuring that a lower entropy corresponds to a more structured and disentangled representation. Disentanglement (D) quantifies whether each estimated latent variable captures at most one true latent factor, computed by applying row-wise entropy over $P_{i,\cdot}$. Completeness (C) assesses whether each true latent factor is captured by a single estimated latent variable, computed via

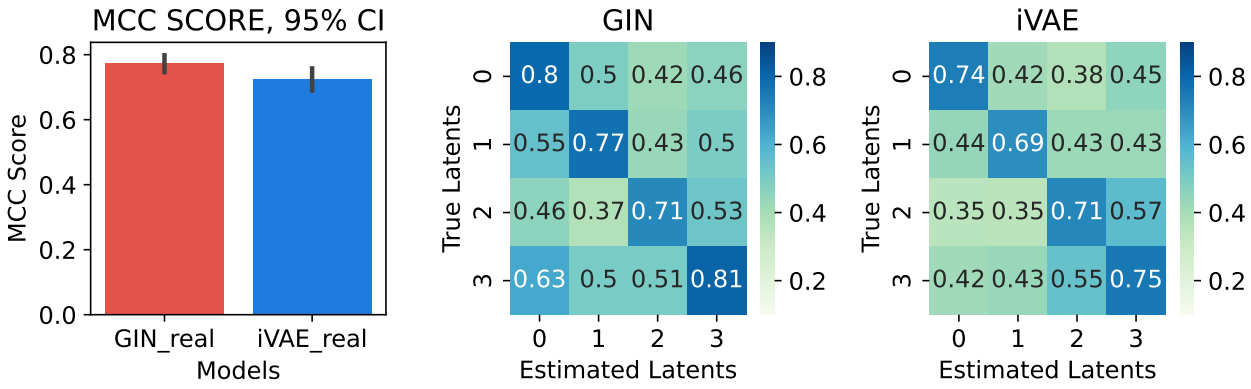

Figure 5: MCC score and mean correlation matrices of GIN and iVAE matched with the best permutation on the setting of Fig. 1b.

column-wise entropy over $P_{\cdot,j}$. Since both scores range from 0 to 1, higher values indicate better structured representations with minimal mixing between factors. All the metrics are measured over 20 repetitions. However, the MCC metric alone is insufficient for measuring the degree of identifiability in scenarios involving partially observable sources since spurious correlation can arise without disentangling the information of $\mathbf{z}_o$ due to the information from the auxiliary variable $\mathbf{z}_o$ being entangled with the observation $\mathbf{x}$.

Additionally, the Fig. 5 demonstrates the insufficiency of MCC score in evaluating the degree of identifiability. The MCC scores of the GIN and iVAE models are around 0.7, suggesting that they recover the true latents reasonably well. However, examining the correlation matrix reveals that the estimated latents also show high correlations with dimensions other than the one with the highest correlation. This is because existing methods do not account for cases where the mixing function includes auxiliary variables, leading to information from the auxiliary variables being entangled in the estimated latents.

Accordingly, we leverage the DCI metric (Eastwood & Williams, 2018) to evaluate whether the learned representation correctly models the conditional independence structure of the graph without spurious correlation. The DCI metric evaluates the performance of disentanglement, completeness, and informativeness of representation by measuring the entropy of the importance matrix (in our case, a MCC matrix) If the true sources are well identified without spurious correlation, the representation will be highly disentangled with complete information.

Data Reflecting the setup of observable sources, we consider synthetic datasets generated from the three graphs in Fig. 1: $\mathcal{D} = \{(\mathbf{x}^{(i)}, \mathbf{z}_o^{(i)})\}_{i=1}^N$, where N is the sample size and $\mathbf{z}_o^{(i)}$ is the observed sources corresponding to the data point $\mathbf{x}^{(i)}$. When we run our selection procedure given a graph to choose the best combination of the auxiliary variables, $\mathbf{z}_o$ will be partitioned into $\mathbf{z}_u$ and $\mathbf{z}_n$.

The data was generated using a linear Structural Causal Model (SCM) where each variable is determined by a linear combination of its parents and an additive noise term:

$$X_i = \sum_{j \in \text{pa}(X_i)} \beta_{ij} X_j + \varepsilon_i, \tag{16}$$

where β_{ij} are sampled uniformly from $[0.5, 1.0]$, and ε_i is the additive noise term with coefficient fixed to 1.0.

To further demonstrate the effectiveness of our method on high-dimensional data, we used the Pendulum and modified Flow datasets Yang et al. (2021), which consist of structured, systematically sampled image data. Corresponding latent causal graphs are shown in Fig. 2.

The implementation of the experiments is based on Liang et al. (2023). Following tables are hyperparameters for learning Ours, GIN and iVAE.

E. Additional Experiments

Table 1: Hyperparameters for different models.

Ours	
LR scheduler	Cosine
Learning rate	0.01
Number of flows	8
Optimizer	Adam
Batch size	1024
Training epochs	20

(a) Synthetic data

GIN	
LR scheduler	-
Learning rate	0.01
Number of flows	8
Optimizer	Adam
Batch size	1024
Training epochs	20

(b) Synthetic data

iVAE	
Number of layers	3
Learning rate	0.0001
Hidden dim	4096
Optimizer	Adam
Batch size	32
Training epochs	20

(c) Synthetic data

Ours	
LR scheduler	Cosine
Learning rate	0.001
Number of flows	8
Optimizer	Adam
Batch size	1024
Training epochs	50

(d) High-dimensional data

GIN	
LR scheduler	-
Learning rate	0.001
Number of flows	8
Optimizer	Adam
Batch size	1024
Training epochs	40

(e) High-dimensional data

iVAE	
Number of layers	3
Learning rate	0.0001
Hidden dim	4096
Optimizer	Adam
Batch size	1024
Training epochs	80

(f) High-dimensional data

Effectiveness of selection We conducted an ablation study on the selection procedure for our architecture. The experiments are based on the data-generating process illustrated in Fig. 2b, where the differences in results arise depending on the selection procedure. Fig. 6 shows the change in DCI metric for our model before and after selection. The selection procedure improves disentanglement in the representation as shown in Fig. 6. For the graph in Fig. 2b, using all observed sources as auxiliary variables without a selection procedure breaks the conditional independence between **Water Height** and **Hole**, leading to entangled representations.

Effectiveness of architecture To verify the effectiveness of our proposed architecture, we choose GIN (Sorrenson et al., 2020) and iVAE (Khemakhem et al., 2020) as baseline models. GIN is used as the encoder in our architecture, ensuring the volume-preserving property but not designed to handle observed sources. iVAE is also not designed to handle partially observed sources. Furthermore, it does not impose any constraints on the mixing function and solely relies on a multivariate normal distribution as the prior, ensuring that each latent variable is conditionally factorizable. For a fair comparison, all experiments are conducted using the same auxiliary variables filtered through the selection procedure.

Fig. 3 demonstrates that our proposed method outperforms other approaches in terms of the DCI metric. Our proposed method maximizes the likelihood of a conditionally factorizable distribution for the remaining components while simultaneously excluding the information of auxiliary variables mixed with the observation $\mathbf{x}$. This prevents spurious correlations in the representation by ensuring that the information of $\mathbf{z}_u$, which is related to unobserved latents, does not mix into the representation.

We further analyzed the results with the MCC matrix for a more detailed examination. The proposed architecture shows a comparable MCC score (mean of diagonal terms) as GIN and iVAE, as illustrated in Fig. 7 for the DGP of Fig. 1a. However, looking at the MCC matrix, we can observe that both GIN and iVAE show high correlations with the other latents besides the true latent, even when matched with the best permutation. This suggests that manipulating a specific dimension of the representation simultaneously affects other latents, indicating that the representation is not well disentangled.

Considering the DGP in Fig. 1b, the ideal disentanglement is that $\hat{z}_1$, $\hat{z}_2$, ($\hat{z}_3$, and $\hat{z}_4$) are conditionally independent. The result of our architecture for MCC matrix in Fig. 8 represents the almost ideal disentanglement, while the other methods still show entangled results. As the conditional independence in DGP in Fig. 1b does not ensure each latent to be identified, but block-identified, the MCC score might be lower. Even in this case, GIN and iVAE, which do not consider observed sources, show a high MCC score because of spurious correlation. Likewise, on the DGP (Fig. 1c), our architecture yields a disentangled MCC matrix as expected.

High-Dimensional data We also conduct the experiments on the Pendulum and Flow datasets from Yang et al. (2021). The images are generated by a latent mechanism shown in Fig. 2. The images have a size of $4 \times 96 \times 96$. For the Flow

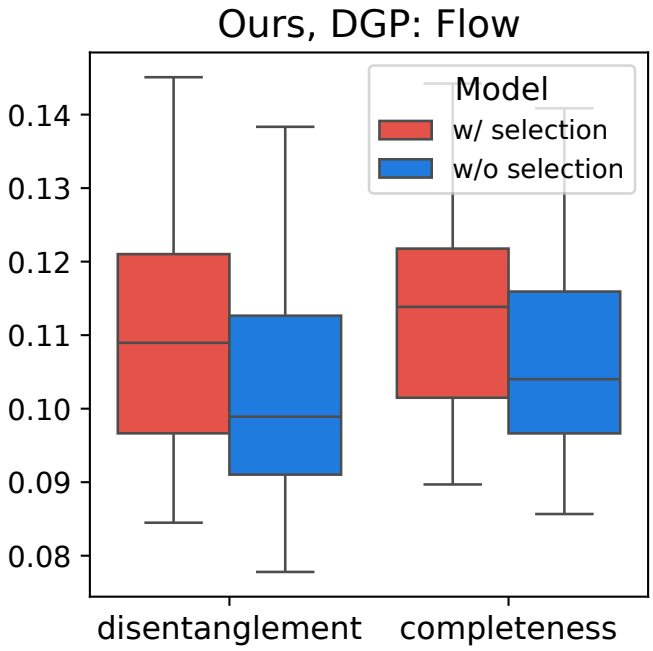

Figure 6: Ablation study on the selection procedure for Ours.

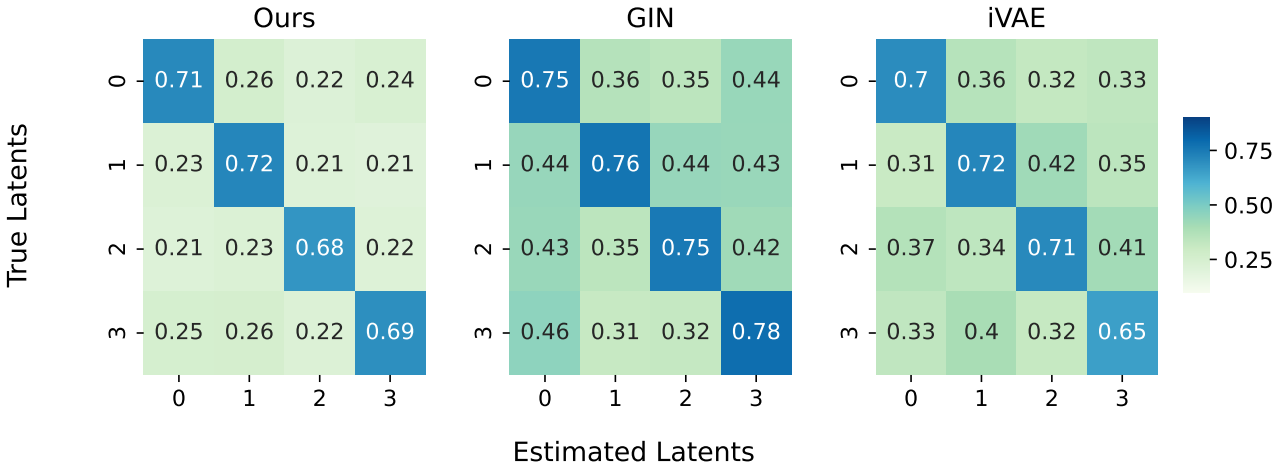

Figure 7: Mean correlation matrices of Ours, GIN applying selection, and iVAE applying selection matched with the best permutation on the setting of Fig. 1a.

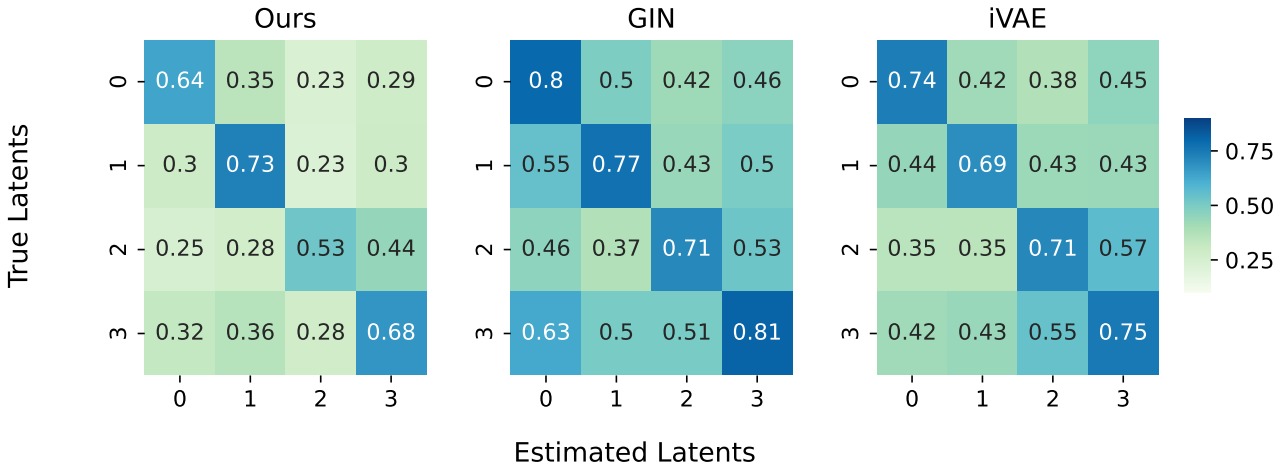

Figure 8: Mean correlation matrices of Ours, GIN applying selection, and iVAE applying selection matched with the best permutation on the setting of Fig. 1b.

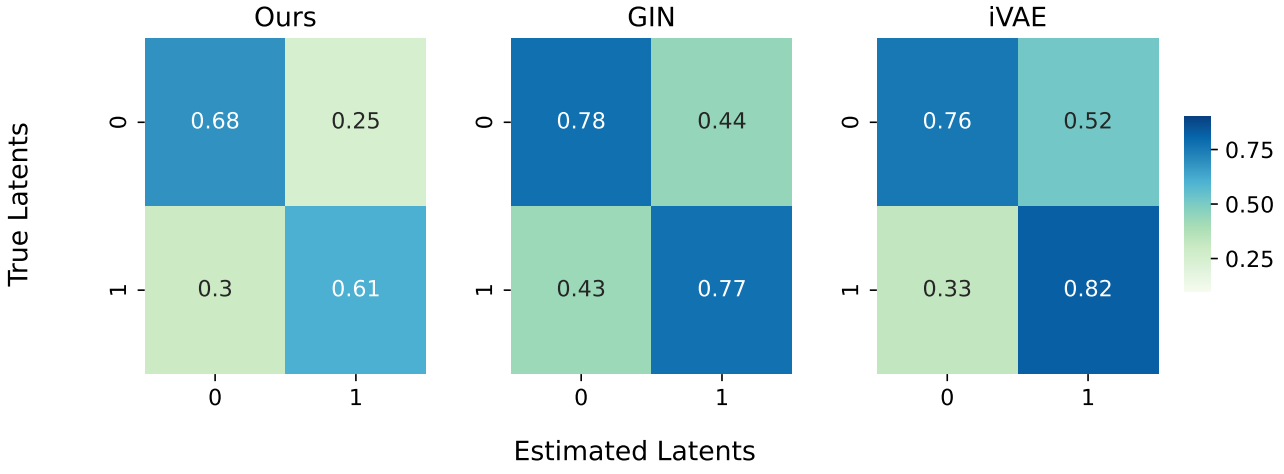

Figure 9: Mean correlation matrices of Ours, GIN applying selection and iVAE applying selection matched with the best permutation on the setting of Fig. 1c.

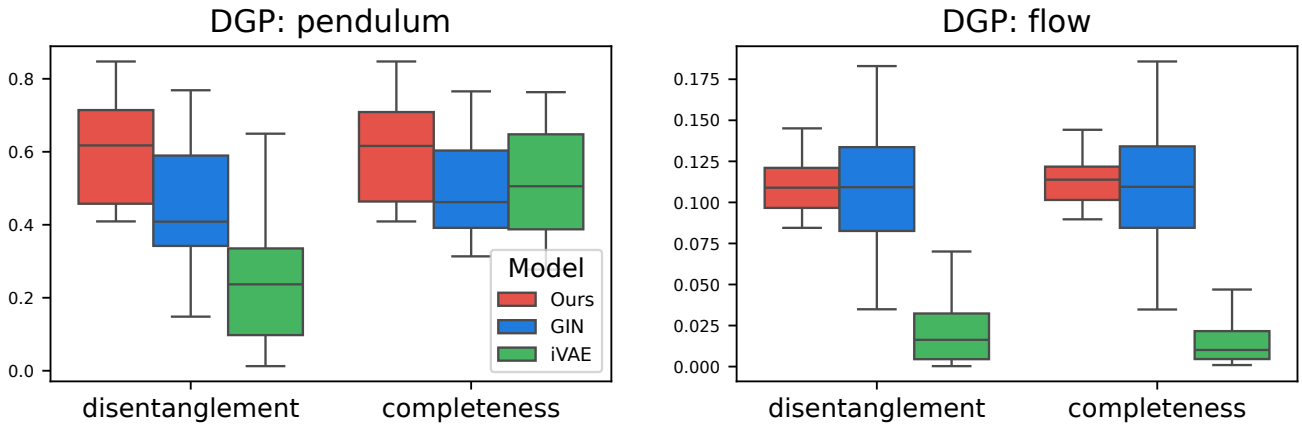

Figure 10: Comparison plot for DCI metric between Ours, GIN , and iVAE on high-dimensional data.

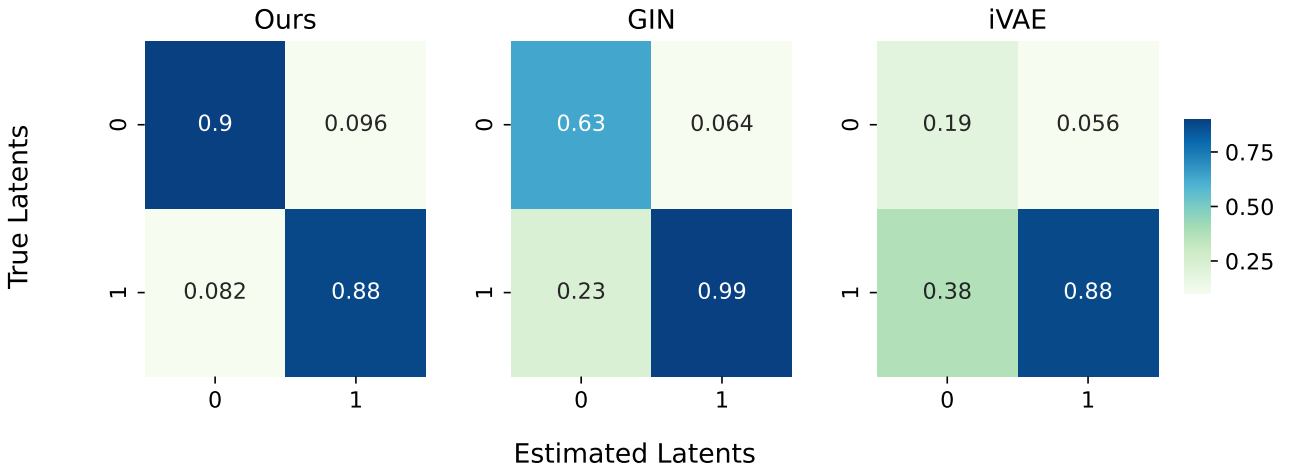

Figure 11: Mean correlation matrices of Ours, GIN applying selection and iVAE applying selection matched with the best permutation on the Pendulum dataset.

dataset, the auxiliary variable **Ball Size** is determined through the selection process. In the case of the Pendulum dataset, all observed latents should be selected as auxiliary variables to ensure the conditional independence of the unobserved latent variables.

As illustrated in Fig. 10, our proposed method demonstrated performance that is comparable to or superior to other models. Unlike the results on synthetic data, the GIN model exhibited strong performance because its normalizing flow-based architecture is more suitable for handling image data in terms of model capacity. The MCC matrices (Figs. 11 and 12) also show that our method learns disentangled representations for unobserved latent variables. It suggests that the learned representations align well with the conditional independence structure of the underlying latent graph in Figs. 2a and 2b.

We also observed that the representations in Flow were more entangled compared to Pendulum. There exists an observed but unselected variable z_n (**Water Flow**), which introduces additional graph constraints. The graph constraints may conflict with the term enforcing conditional independence, making the learning process more challenging. Addressing this challenge remains an avenue for future work.

E.1. Latent Traverse

For better comprehensibility, we further extend our model to the image reconstruction task and perform latent traversal to assess whether the factors have been disentangled effectively. We conducted experiments on the pendulum dataset as shown

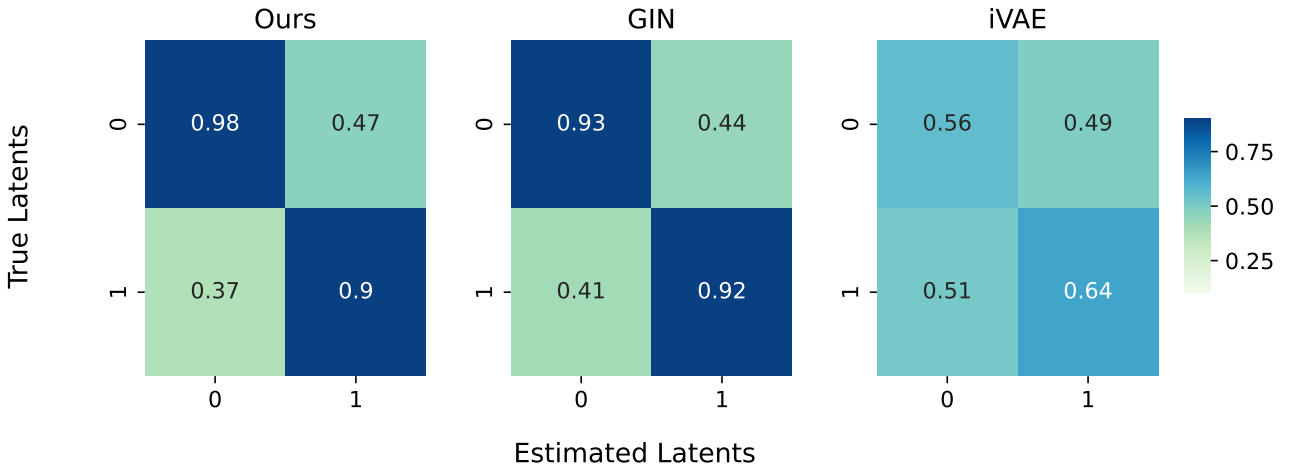

Figure 12: Mean correlation matrices of Ours, GIN applying selection and iVAE applying selection matched with the best permutation on the Flow dataset.

in Fig. 2a, choosing the pendulum angle and light position as selected variables. To efficiently extract relevant features from high-dimensional image data and visualize disentangled factors, an extra encoder-decoder architecture with an additional MSE (Mean Squared Error) loss was adopted to ensure successful compression and reconstruction of the images.

The encoder comprises four 2D convolutional layers followed by two fully connected layers with ReLU activation. It compresses the input data into exogenous latent variables corresponding to the number of nodes in the causal graph. These set of variables are then passed through our model, generating endogenous latent variables of the same dimensionality. The decoder adopts a scene-mixture approach, which is widely used in object-centric representation learning. Specifically, each scalar value from the endogenous latent variables passes through six fully connected layers, producing full-size image arrays that are subsequently averaged to reconstruct the final image. Empirical results indicate that the scene-mixture approach enhances the effectiveness of latent traversal compared to a single decoder with a similar number of parameters.

Fig. 4 presents the results of generating counterfactual images by traversing unobserved latent variables after training our model with the reconstruction objective. As shown in the upper row, traversing the variable associated with shadow length gradually decreases its extent in the reconstructed images. Similarly, modifying the latent variable corresponding to shadow position causes the shadow to shift progressively to the right while mostly preserving the other factors. The successful disentanglement of unobserved latent variables further demonstrates the model's effectiveness in its transferability.

Algorithm 3 Bayes Ball Algorithm for d-connected nodes

Input: Graph G, Conditioning Set C, Observed Set O, Set of nodes R
Output: Updated set of d-connected nodes R
Initialize an empty set V FOR visited nodes
Initialize an empty queue Q
for each node n in R **do**
  Add (n, up) to Q
end for
while Q is not empty **do**
  $(node, direction) \leftarrow Q.pop()$
  if $node \in V$ **then**
    continue
  end if
  Add $node$ to V
  if $node \in C$ **and** $direction \neq$ down **then**
    continue
  end if
  if $direction =$ up **then**
    for each $parent$ of $node$ in G **do**
      Add $(parent, \text{up})$ to Q
    end for
    for each $child$ of $node$ in G **do**
      Add $(child, \text{down})$ to Q
    end for
  else if $direction =$ down **then**
    Initialize $check \leftarrow$ false
    for each descendant d of $node$ in G **do**
      if $d \in C$ **then**
        $check \leftarrow$ true
        break
      end if
    end for
    if $node \in C$ **or** $check =$ true **then**
      for each $parent$ of $node$ in G **do**
        Add $(parent, \text{up})$ to Q
      end for
    else
      for each $child$ of $node$ in G **do**
        Add $(child, \text{down})$ to Q
      end for
    end if
  end if
  if $node \notin C$ and $node \notin O$ **then**
    Add $node$ to R
  end if
end while
return R